Mechanism of Microsomal Epoxide Hydrolase. Semifunctional Site-Specific Mutants Affecting the Alkylation Half-Reaction†

L. Timothy Laughlin, Huey-Fen Tzeng, Sue Lin, and Richard N. Armstrong*

Departments of Biochemistry and Chemistry and Center in Molecular Toxicology, Vanderbilt University School of Medicine, Nashville, Tennessee 37232-0146

Received November 5, 1997; Revised Manuscript Received January 5, 1998

ABSTRACT: Microsomal epoxide hydrolase (MEH) catalyzes the addition of water to epoxides in a two-step reaction involving initial attack of an active site carboxylate on the oxirane to give an ester intermediate followed by hydrolysis of the ester. An efficient bacterial expression system for the enzyme from rat that facilitates the production of native and mutant enzymes for mechanistic analysis is described. Pre-steady-state kinetics of the native enzyme toward glycidyl-4-nitrobenzoates, **1**, indicate the rate-limiting step in the reaction is hydrolysis of the alkyl-enzyme intermediate. The enzyme is enantioselective, turning over (2*R*)-**1** about 10-fold more efficiently than (2*S*)-**1**, and regiospecific toward both substrates with exclusive attack at the least hindered oxirane carbon. Facile isomerization of the monoglyceride product is observed and complicates the regiochemical analysis. The D226E and D226N mutants of the protein are catalytically inactive, behavior that is consistent with the role of D226 as the active-site nucleophile as suggested by sequence alignments with other α/β-hydrolase fold enzymes. The D226N mutant undergoes hydrolytic autoactivation with a half-life of 9.3 days at 37 °C, suggesting that the mutant is still capable of catalyzing the hydrolytic half-reaction (in this instance an amidase reaction) and confirming that D226 is in the active site. The indoylyl side chain of W227, which is in or near the active site, is not required for efficient alkylation of the enzyme or for hydrolysis of the intermediate. However, the W227F mutant does exhibit altered stereoselectivity toward (2*R*)-**1**, (2*S*)-**1**, and phenanthrene-9,10-oxide, suggesting that modifications at this position might be used to manipulate the stereo- and regioselectivity of the enzyme.

Microsomal epoxide hydrolase (MEH)[1] (EC 3.3.2.3) catalyzes the addition of water to epoxides and arene oxides generated by the cytochrome P450-catalyzed oxidation of unsaturated hydrocarbons (*1*). The reaction mechanism involves two steps, initial attack of an active-site carboxylate at one of the oxirane carbons of the substrate to give an alkyl-enzyme (ester) intermediate and the subsequent hydrolysis of the intermediate by attack of water at the carbonyl carbon of the ester (*2*). The minimal kinetic mechanism of the enzyme is shown in eq 1 where rapid equilibrium binding (K_s) of the substrate to form a Michaelis complex is followed by reversible formation (k_2/k_{-2}) and essentially irreversible hydrolysis (k_3) of the intermediate (E−I).

$$E + S \overset{K_s}{\rightleftharpoons} E{\cdot}S \underset{k_{-2}}{\overset{k_2}{\rightleftharpoons}} E{-}I \xrightarrow{k_3} E + P \qquad (1)$$

For most substrates, the rate-limiting step in the enzyme-catalyzed reaction is hydrolysis of the intermediate (*3*).

Microsomal epoxide hydrolase is a member of the α/β-hydrolase fold family of enzymes. This family is an evolutionarily divergent group of hydrolases with a catalytic triad consisting of a nucleophile (Ser, Cys, or Asp) for formation of either an acyl- or an alkyl-enzyme intermediate, a general base (His), and a charge relay residue (Asp or Glu) for hydrolysis of the intermediate (*4*). The catalytic triads of all are arranged in the following sequence: nucleophile, charge relay acid, general base. Although there is very little experimental evidence as to the identity and function of active-site residues in MEH, detailed proposals have been advanced based on regions of high-sequence similarity with haloalkane dehalogenase, for which there is a high-resolution crystal structure, soluble epoxide hydrolase, and other members of the α/β-hydrolase fold family of enzymes (*2*, *5*−*8*). Sequence alignments clearly identify D226 of MEH as the nucleophile in formation of the ester. Although somewhat less clearly, the alignments also indicate that H431 acts as the general base in the hydrolytic half-reaction, an observation consistent with the earlier finding by Bell and Kasper (*9*) that H431 is essential for catalysis.

A proposed active site for MEH based on sequence alignments and other considerations is illustrated in Figure 1. In principle, a two-step mechanism provides the opportunity to dissect the roles of specific residues in catalysis through the construction of semifunctional mutants that are

† This work was supported in part by NIH Grants R01 GM49878, P30 ES00267, and T32 ES07028. L.T.L. is supported by NRSA Fellowship F32 GM18296 from the National Institute of General Medical Sciences.

* Address correspondence to this author. Phone: (615) 343-2920. FAX: (615) 343-2921. Email: armstrong@toxicology.mc.vanderbilt.edu.

[1] Abbreviations: MEH, microsomal epoxide hydrolase; MOPS, 3-(*N*-morpholino)propanesulfonic acid; CD, circular dichroism; NMR, nuclear magnetic resonance; PCR, polymerase chain reaction; LB, Luria broth; OD, optical density; PEG, poly(ethylene glycol) 6000; dNTP, deoxynucleotide triphosphate; HPLC, high performance liquid chromatography; ppm, parts per million; SDS−PAGE, sodium dodecyl sulfate−polyacrylamide gel electrophoresis.

S0006-2960(97)02737-2 CCC: $15.00
Published on Web 02/07/1998

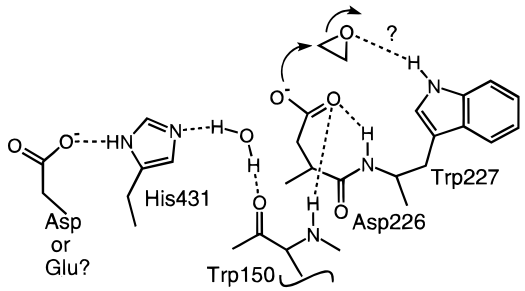

FIGURE 1: Proposed active site for microsomal epoxide hydrolase based on sequence alignments with other α/β-hydrolase fold enzymes (*2*, *7*, *8*) and the three-dimensional structure of haloalkane dehalogenase (*5*). The enzyme is shown poised for the alkylation half-reaction.

Scheme 1

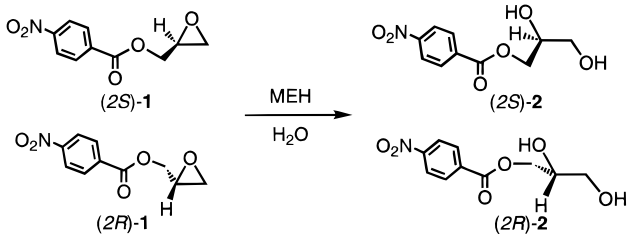

dysfunctional in only one of the two half-reactions. That the hydrolysis of the alkyl-enzyme is rate-limiting allows the effects of mutations on individual steps to be examined by a combination of pre-steady-state and steady-state kinetics. So, for example, if W227 is involved in activation of the oxirane as suggested in Figure 1, mutation of this residue would be expected to slow the alkylation reaction but have little influence on hydrolysis of the ester. Similarly, it is anticipated that if the unknown charge relay carboxylate was mutated, then the alkylation reaction would be unaffected and the hydrolysis half-reaction slowed.

In this paper, we describe, in detail, a pre-steady-state kinetic analysis of native and mutant MEH from rat toward the two enantiomers of glycidyl-4-nitrobenzoate, **1** (Scheme 1). The enzyme exhibits a significant enantioselectivity toward **1** which is primarily manifest in the hydrolysis half-reaction. The regiospecificity of the alkylation half-reaction for both (2*R*)- and (2*S*)-**1** is established, by isotopic labeling of the product, as attack of the carboxylate at the primary oxirane carbon. The specific roles of residues thought to participate in the alkylation half-reaction of the catalytic mechanism are revealed through the construction of semi-functional site-specific mutants. The results indicate that D226 is the active site nucleophile alkylated in the first half-reaction and suggest that the indoylyl NH of W227 is not involved in activating the oxirane of the substrate for nucleophilic attack. The side chain at position 227 does influence the stereoselectivity of the enzyme. A preliminary report of a portion of this work has appeared (*3*).

EXPERIMENTAL PROCEDURES

General Materials and Methods. The (2*R*)- and (2*S*)-enantiomers of glycidyl-4-nitrobenzoate, **1,** were from Aldrich. Phenanthrene 9,10-oxide, **3**, was synthesized as previously described (*10*). Water enriched in ^{18}O (67−70%) was from Isotec. All buffer salts, chemical reagents, solvents, enzymes, and media were of the highest quality commercially available. The detergent Genapol C-100 was obtained from Calbiochem. Oligonucleotides were synthesized in the Center in Molecular Toxicology Core Lab at Vanderbilt or purchased from GIBCO−BRL. The pET20 plasmid was from Novagen (Madison, WI). Vent DNA polymerase, T4 DNA ligase, and restriction endonucleases were purchased from New England Biolabs (Beverly, MA). Peptone and yeast extract were supplied by GIBCO−BRL (Bethesda, MD). The concentrations of purified epoxide hydrolase and the W227F mutant were measured spectrophotometrically at 280 nm using calculated extinction coefficients of 80 400 M^{-1} cm^{-1} (*2*) and 75 920 M^{-1} cm^{-1}, respectively. Proton and ^{13}C NMR spectra were obtained on a Bruker AC300 spectrometer with a multinuclear probe housed in the Vanderbilt Department of Chemistry NMR Facility.

Construction of Expression Vectors. The PCR technique was employed to amplify the coding region of epoxide hydrolase out of plasmid pEH52 (*11*). The following primers were used: 5′ primer, AAA CTC GAG GTC GAC ACA TAT GTG GCT GGA ACT TGT CCT GGC; 3′ primer, AAA GAA TTC GTC GAC CTA CTG CAG CTC AGC CAG GGA CAC. The primers were designed to place an *Nde*I restriction site immediately 5′ to the start codon and an *Eco*RI site immediately 3′ to the stop codon. Forty cycles consisting of 45 s at 94 °C, 45 s at 60 °C, and 2 min at 72 °C were run using 100 ng of pEH52, 100 μM of each primer, 400 μM of each nucleoside triphosphate, and 2 units of Vent DNA polymerase. The PCR product was extracted into 20 μL of TE buffer using the Wizard Miniprep method (Promega). The PCR product and the plasmid pET20 were each digested with the restriction endonucleases *Nde*I and *Eco*RI and subsequently purified in a low melting point agarose gel. The plasmid and the epoxide hydrolase coding region were extracted out of gel slices and ligated together. The resulting construct was designated pET20MEH1.

Expression and Purification of Epoxide Hydrolase. BL21-(DE3) cells were transformed with pET20MEH1 and plated out on LB−ampicillin (200 μg/mL) plates. The colonies were not allowed to grow larger than 1 mm diameter. A colony was picked and used to inoculate 1 L of LB media supplemented with 100 μg/mL ampicillin. The starter culture was grown at 37 °C until the OD_{600} reached 0.2. The starter was used to inoculate 10 L of LB−ampicillin (100 μg/mL) in a fermentor (Bioflow 2000, New Brunswick), which was grown until the OD_{600} reached 1.2, at which time 10 g/L lactose was added. The culture was grown for an additional 5−8 h before harvesting. The cells were harvested by centrifugation and stored at −20 °C. The cell pellets were resuspended in 0.01 M Tris/HCl, pH 7.6. The suspension was sonicated with four 3 min bursts at 80% power with a Branson Sonifier. The lysate was allowed to cool for 10 min between each burst. The lysate was centrifuged 45 min at 16 000 rpm. The pellets were then extracted twice with 0.01 M Tris/HCl containing 0.5% Genapol C-100 (pH 7.6). The extract was then passed through a DEAE-cellulose column (2.5 × 100 cm) equilibrated with 0.01 M Tris/HCl, 0.1 M KCl, 0.2% Genapol C-100 (pH 7.6). After the extract was loaded, the column was washed with the same buffer. The detergent−epoxide hydrolase complex was a component of the first peak that eluted from the column. The fractions containing epoxide

hydrolase activity were pooled. The enzyme was dialyzed against 0.01 M Tris/HCl (pH 7.6) and loaded onto an hydroxylapatite column (1 × 6 cm). The column was washed with 10 bed volumes of 0.01 M potassium phosphate buffer (pH 7.6). The enzyme was then eluted with 0.5 M potassium phosphate. The enzyme was dialyzed against 0.01 M Tris/HCl (pH 7.6) and concentrated for storage.

Site-Directed Mutagenesis. The Kunkel method (*12*) was employed for creating site-specific mutations in the MEH coding region. Briefly, *E. coli* CJ236 cells were transformed with pET20MEH1. Uracil-containing single-stranded pET20MEH1 DNA was produced by infecting transformed cells with M13K07 helper phage. Phagemid particles containing the DNA were precipitated with PEG, and the DNA was extracted with phenol/chloroform. After precipitation with 2-propanol, the single-stranded template was annealed to a mutagenic primer, the second strand synthesized by T7 DNA polymerase and dNTPs, and the nicked duplex sealed with T4 DNA ligase. The reaction mixture was used to transform DH5α cells and plated onto LB−ampicillin plates. Resulting colonies were screened for the mutation using restriction digests utilizing a silent restriction site incorporated into each mutagenic primer. Positive clones were sequenced throughout the coding region and used to transform BL21(DE3) cells for protein production.

Enzyme Assay and Steady-State Kinetics. The hydration of phenanthrene 9,10-oxide was followed spectrophotometrically at 290 nm ($\Delta\epsilon = -5250\ M^{-1}\ cm^{-1}$) on a Perkin-Elmer Lambda 4B spectrophotometer essentially as described by Armstrong et al. (*13*). All assays were performed at 25 °C. Assay of the enzyme during the various steps of the purification was accomplished by combining 925 μL of buffer (50 mM MOPS, pH 8.0) with 50 μL of a 2 mM solution of phenanthrene 9,10-oxide in CH_3CN, equilibrating the solution for 5 min at 25 °C and initiating the reaction with 25 μL of an appropriate concentration of enzyme. Steady-state kinetic analysis of the enzyme toward (2*R*)-**1** and (2*S*)-**1** was performed by the HPLC method previously described (*3*). Initial velocity data were analyzed by the program HYPER (*14*).

Stopped-Flow Data Acquisition and Analysis. The pre-steady-state and post-steady-state kinetic experiments were conducted on an Applied Photophysics model SX17MV stopped-flow spectrometer operated in the fluorescence mode. Samples were excited at 290 nm through two monochromators, and the total protein fluorescence was observed through a 320 nm cutoff filter. All reactions were performed in 50 mM MOPS (pH 7.0) containing 5% CH_3CN at 25 °C. Enzyme concentrations were typically 3−8 μM and the substrate concentrations were varied between 0.05 and 1.0 mM, the solubility limit. The reported concentrations of reagents are those in the reaction cell. Each kinetic trace was the average of five to eight individual experiments depending on the signal/noise. The pre-steady-state data were fit to the equation $k_{obs} = k_{-2} + k_2[S]/(K_s + [S])$ when saturation was observed and to $k_{obs} = k_{-2} + k_2[S]/K_s$ when no saturation was observed. The kinetics of the post-steady-state recovery of fluorescence were analyzed using the KINSIM (*15*) and FITSIM (*16*) programs to estimate the turnover number, k_3.

Regioselectivity of MEH toward 1. The regioselectivity of the reactions was determined from the distribution of ^{18}O in product isolated from multiple-turnover reactions in the presence of water containing 50 mol % ^{18}O. Reactions of 1−2 mL containing 5−50 μM enzyme and 50 mM substrate added in five equal aliquots over a period of several hours were run to completion at room temperature. The monoglyceride products were extracted with ether and dried over Na_2SO_4. The solvent was evaporated and the product was dried under vacuum before being dissolved in CD_3CN for NMR analysis. The extent of isotope incorporation at the primary and secondary carbons was estimated by ^{13}C NMR spectroscopy from the relative intensities of the ^{13}C resonances located at 63.7, 67.7, and 70.7 ppm and isotope-perturbed (^{13}C-^{18}O) resonances located 0.01−0.03 ppm upfield.

Kinetics of Isomerization of the Product. The monoglyceride products **2** and **4** were separated by chromatography on a 21.4 × 250 mm Microsorb C18 (Rainin) column eluted at 12 mL/min with 30% (v/v) dioxane/water. The two products, **2** (eluting at 15.8 min) and **4** (eluting at 13 min), were collected in flasks immersed in a dry ice/ethanol bath. After lyophilization of the solvent, product **4** was dissolved in 0.05 M MOPS/KOH buffer, (pH 7.0), and the isomerization was monitored by HPLC on a 4.6 × 250 mm Microsorb C18 column (Rainin) using a 45% methanol/55% water solvent system. The observed rate constant for the approach to equilibrium was obtained from the exponential [mol % **4**(t) − mol % **4** (∞)] vs t. The identities of **2** and **4** were established from their ^{13}C and ^1H NMR spectra. **2**: ($CDCl_3$) ^{13}C δ 63.7 ($OCH_2CHOHCH_2OH$), 67.7 ($OCH_2CHOHCH_2$-OH), 70.7 ($OCH_2CHOHCH_2OH$), 123.6 (aromatic C with connected H), 130.9 (aromatic C with connected H), 135, 150.7, 165; ^1H δ 3.6 (m, 2H) ($OCH_2CHOHCH_2OH$), 3.92 (m, 1H) ($OCH_2CHOHCH_2OH$), 4.3 (m, 1H) and 4.4 (m, 1H) ($OCH_2CHOHCH_2OH$), 8.20 (m, 2H), 8.28 (m, 2H). **4**: ($CDCl_3$) ^{13}C δ 61.5 ($OCH(CH_2OH)_2$), 78.3 ($CH(CH_2OH)_2$), 123.6 (aromatic C with connected H), 130.9 (aromatic C with connected H), 135, 150.7, 165; ^1H δ 3.75 (d, 4H, J = 5.6 Hz) ($CH(CH_2OH)_2$), 5.1 (m, 1H) ($CH(CH_2OH)_2$), 8.1 (m, 2H), 8.3 (m, 2H).

Enantiomeric Composition of the Diol Product from Phenanthrene 9,10-Oxide, 3. Enzyme-catalyzed reactions of **3** (100 μM) were run to completion in 5 mM MOPS/KOH buffer (pH 7.0) containing 5% acetonitrile. The dihydrodiol product was extracted using a 3-mL BAKERBOND spe* Octadecyl column (J. T. Baker), eluted, and further purified by reversed-phase HPLC on a Beckman C18 Ultrasphere column (4.6 mm × 25 cm) using a 55% methanol/45% water solvent system. The enantiomeric composition of the 9,10-dihydroxy-9,10-dihydrophenanthrene was determined directly from the CD spectrum of the purified product on a JASCO J-720 spectropolarimeter.

RESULTS

Heterologous Expression and Purification of Epoxide Hydrolase. Expression of the native enzyme in *E. coli* BL21(DE3) cells harboring the pET20MEH1 plasmid was accomplished with sufficient yield for extensive mechanistic study. To the best of our knowledge this is the first report of a prokaryotic expression system for *native* MEH and compliments the original bacterial expression system of an active OmpA leader sequence−MEH fusion protein (*9*). The simple three-step purification scheme allows production of

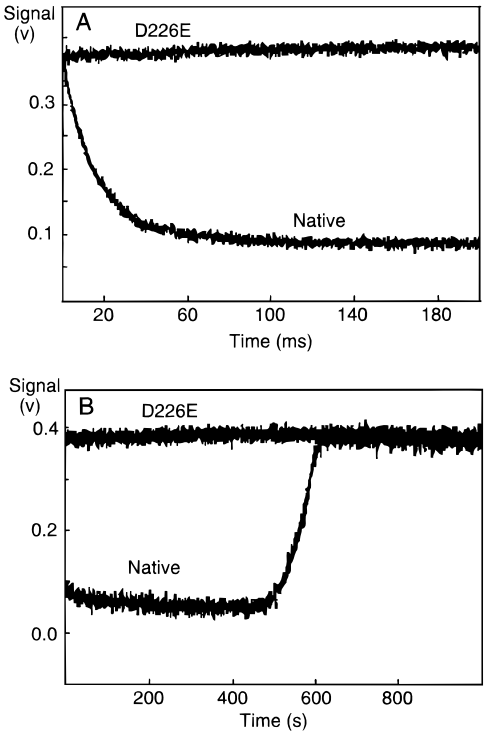

FIGURE 2: (A) Pre-steady-state decrease in the intrinsic fluorescence of MEH (5.0 μM) when mixed with 250 μM (2*R*)-**1** at 25 °C (pH 7.0). Each trace is an average of five reactions. The decrease follows a single exponential with $k_{obs} = 15$ s^{-1}. (B) Post-steady-state recovery of fluorescence upon consumption of the substrate. The upper trace in both panels is for the D226E mutant under identical conditions.

detergent-free MEH and mutants more quickly and at a lower cost than the previously reported baculoviral expression system (*17*). Typically, 1.5 mg of purified MEH was recovered from each liter of cell culture after a simple three-step purification. The enzyme from typical preparations was greater than 90% pure as estimated from SDS−PAGE and had k_{cat} values between 0.9 and 1.1 s^{-1} toward phenanthrene 9,10-oxide that compare favorably with epoxide hydrolase isolated from rat liver microsomes and other expression systems (*2*, *13*, *17*, *18*).

Pre-Steady-State Kinetics of the Native Enzyme. Rapid mixing of MEH with a large excess of either (2*R*)-**1** or (2*S*)-**1** results in quenching of the intrinsic protein fluorescence as shown in Figure 2. The rapid decrease in fluorescence follows a single exponential until a steady-state level is reached and, in the post-steady-state phase, recovers to the original level upon consumption of substrate. The observed first-order rate constant (k_{obs}) for the fluorescence decrease as well as the duration of the subsequent steady-state phase is dependent on the concentration of the substrate. Higher concentrations of substrate increase k_{obs} and the time required for recovery of the original fluorescence.

The concentration dependence of the pre-steady-state fluorescence decay allows an evaluation of the rate constants leading to the formation of the ester intermediate. The rate of fluorescence quenching exhibits saturation behavior with (2*R*)-**1** allowing the determination of the rate constants k_2, k_{-2}, and K_s (Table 1) for this substrate as defined in eq 1. The saturation behavior observed with the R-enantiomer suggests that the fluorescence quenching is not caused by formation of the Michaelis complex but by a subsequent step that precedes the rate-limiting step. Although the magnitude of the pre-steady-state fluorescence change with the enantiomer (2*S*)-**1** is the same as with (2*R*)-**1**, k_{obs} does not show saturation behavior. As a consequence, only lower limits for k_2 and K_s can be obtained for (2*S*)-**1** (Table 1). The relative efficiency of alkylation by both substrates can be evaluated by comparison of the apparent second-order rate constants (k_2/K_s) for formation of the intermediate from free enzyme and substrate and is found to be similar (Table 1). Perhaps the most interesting observation in the pre-steady state for either substrate is that the formation of the ester is reversible ($k_{-2} > 0$).

The turnover number of the enzyme (k_3) estimated from the lag and the post-steady-state recovery of fluorescence (Figure 2) is much lower than the rate constant for alkylation and in good agreement with that determined by classical steady-state measurements (Table 1) such that $k_3 = k_{cat}$. Thus, in the steady state, virtually all of the enzyme is alkylated. It is also interesting to note that turnover to product is slower than decomposition of the ester to enzyme-bound substrate ($k_{-2} > k_3$). Finally, the enantioselectivity of the enzyme is manifest in the hydrolysis half-reaction where k_3 values for the two enantiomers differ by a factor of 10. In fact, the rate constants for both decomposition pathways of the alkyl-enzyme intermediate (k_{-2} and k_3) are both an order of magnitude smaller for (2*S*)-**1**, suggesting that this ester is, for whatever reason, more stable.

Regioselectivity of the Native Enzyme. The hydration of **1** can occur by initial attack of the enzyme at either the 1°- or 2°-position of the oxirane to give one, the other or a mixture of isomeric esters. In principle, the regiochemistry of the reaction can be ascertained either from the stereochemical composition of the diol product, **2**, or by tracking the incorporation of isotopically enriched water in the product. In fact, the facile rearrangement of the monoglycerides scrambles the stereochemical outcome (*19*), leaving isotopic labeling the option of choice (Scheme 2). The regiochemistry was determined from the ^{18}O distribution in **2** isolated from multiple turnover reactions of both (2*R*)- and (2*S*)-**1** in 50% $H_2{}^{18}O$. Of the ^{13}C signals for C1, C2, and C3 (Figure 3) at 67.7, 70.7, and 63.7 ppm, respectively, only the signals for the terminal carbons at 63.7 and 67.7 ppm exhibited an isotopically perturbed peak upfield of the parent (Figure 3). The isotope is distributed equally between both terminal carbons resulting in an intensity of the ^{18}O-perturbed signal one-third that of the parent. This result is consistent with exclusive (>95%) nucleophilic attack at the least hindered carbon with the appearance of ^{18}O at the C1 carbon due to acyl migration of the nitrobenzoyl group during the reaction and workup.

Evidence for the acyl migration includes the detection of the intermediate product **4** by NMR spectroscopy and its isolation by HPLC. For example, the ^{13}C signals for normal and isotopically perturbed primary carbons of **4** are clearly visible at 61.5 ppm in Figure 3. When **4** was incubated under the conditions of the enzyme-catalyzed reactions, it isomerized to an equilibrium mixture of 92.7% **2** and 7.3% **4** with a half-life of 6.4 min, a time much shorter than that required for reaction and workup. The ratio of the two products is typical of that observed for other monoglycerides (*19*). The observed rate constant for the approach to equilibrium was 1.8×10^{-3} s^{-1} at 25 °C and pH 7.

Table 1: Pre-Steady-State and Steady-State Kinetic Constants for the Enzyme-Catalyzed Hydration of the Enantiomers of **1**

enzyme/ substrate	pre/post steady state[a]					steady state[b]	
	k_2 (s^{-1})	k_{-2} (s^{-1})	K_s (mM)	k_2/K_s (M^{-1} s^{-1})	k_3 (s^{-1})	k_{cat}/K_m (M^{-1} s^{-1})	k_{cat} (s^{-1})
native[c]							
(2*R*)-**1**	330 ± 50	4.0 ± 1.8	2.0 ± 0.5	(1.7 ± 0.3) × 10^5	0.8 ± 0.1	(3.0 ± 0.8) × 10^4	0.57 ± 0.07
(2*S*)-**1**	>250	0.45 ± 0.13	>3	(1.1 ± 0.1) × 10^5	0.07 ± 0.01	(1.5 ± 0.2) × 10^4	0.057 ± 0.006
W227F							
(2*R*)-**1**	>250	3.4 ± 0.4	>3	(4.1 ± 0.1) × 10^4	0.9 ± 0.1	(0.8 ± 0.2) × 10^4 [d]	ND
(2*S*)-**1**	>250	1.4 ± 0.3	>3	(5.0 ± 0.1) × 10^4	0.56 ± 0.01	(1.4 ± 0.1) × 10^4 [d]	ND

[a] Values of k_2, k_{-2}, K_s, and k_2/K_s were obtained from the dependence of k_{obs} on the concentration of substrate (for example, see Figure 5). Values of k_3 were obtained from fitting the pre-steady-state and post-steady-state lag phase (Figure 2B) by numerical integration of the kinetic mechanism (eq 1). [b] Obtained from the substrate dependence of initial velocities. ND = not determined. [c] Data from (*3*). [d] Calculated from the relationship $k_{cat}/K_m = (k_2/K_s)[k_3(/k_3 + k_{-2})]$.

Scheme 2

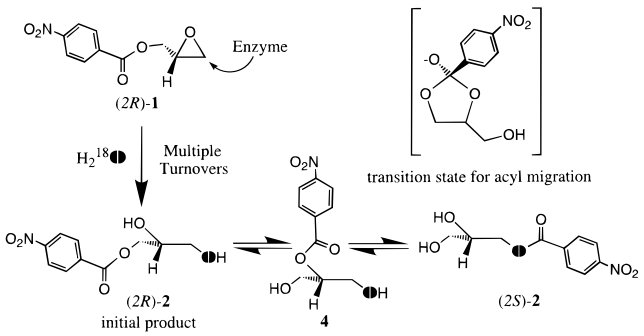

Catalytic and Chemical Properties of D226 Mutants. The proposal that D226 is the active-site nucleophile was tested by making the D226E and D226N mutants. Both mutants were expressed in good yield using the appropriately modified pET20MEH1 vector. Purification was accomplished by the procedure used for the native enzyme without modification. Neither mutant exhibited detectable catalytic activity toward **1** or **3**. Moreover, the D226E mutant showed no change in fluorescence on incubation with (2*R*)-**1** either in the stopped flow or for more extended periods of time as shown in Figure 2, indicating that it fails to undergo alkylation as does the native enzyme. This observation also supports the suggestion that the rapid initial decrease in fluorescence of the native enzyme when mixed with **1** is not due to formation of a Michaelis complex.

Incubation of D226N for extended periods of time at pH 8.0 and 37 °C results in the slow ($t_{1/2}$ = 9.3 days) autoactivation of the mutant to give essentially fully active enzyme as illustrated in Figure 4. The native enzyme is remarkably stable under the same conditions, losing less than 15% of its original activity over a period of 30 days. Do the residues normally involved in the hydrolytic half-reaction accelerate the hydrolysis of the amide? For comparison, the pentapeptide GGNWG has an estimated half-life of ≥60 days at pH 7.5 and 37 °C (*20*). Thus, the autoactivation of D226N appears to be accelerated about 6-fold in the environment of the active site compared to the hydrolysis of the side chain amide of an asparagine in a sequence context identical to that in D226N.

Properties of the W227F Mutant. To determine whether the indoylyl-NH of W227 participates in the alkylation half-reaction (Figure 1), the W227F mutant was prepared. The mutant was expressed and isolated in good yield using the pET20MEH1 vector and the standard purification protocol. The mutant enzyme exhibited a slightly enhanced turnover number of 2.2 s^{-1} with **3**. In addition, the pre-steady-state kinetic constants for the alkylation half-reaction with both (2*R*)- and (2*S*)-**1** were close to those determined for the native enzyme (Table 1), suggesting that indoylyl-NH of W227 does not participate in the alkylation as suggested in Figure 1. The only difference is that saturation behavior cannot be detected with either substrate in the accessible concentration range. In addition, the replacement of W227 with phenylalanine does not significantly affect the fluorescence change observed upon alkylation, suggesting that other tryptophan residues (e.g., W150, Figure 1) are involved in the spectral change.

The mutation is not without effect on the reaction. In contrast to the native enzyme, the turnover numbers for the W227F mutant toward (2*R*)-**1** and (2*S*)-**1** differ by a factor of less than 2: 0.9 s^{-1} and 0.56 s^{-1}, respectively. Thus, the enantioselectivity observed in the hydrolysis half-reaction is considerably less than that of the native enzyme. The regioselectivity toward the enantiomers of **1** as determined by ^{18}O labeling remains the same, exclusive (>95%) attack at the primary carbon.

The hydration of the *meso*-epoxide, **3**, can yield two enantiomers depending on whether the attack occurs at the oxirane carbon of *R* or *S* absolute configuration (Scheme 3). The stereoselectivity is a consequence solely of the alkylation half-reaction. The native enzyme is barely able to distinguish between the two enantiotopic carbons and gives a 60/40 mixture of the dihydrodiols (*9S,10S*)-**5** and (*9R,10R*)-**5** (*21*). The stereoselectivity of the W227F mutant is slightly higher, producing a 75/25 mixture of (*9S,10S*)-**5** and (*9R,10R*)-**5**. Although W227 does have a detectable effect on the alkylation half-reaction, it is clear the specific interaction suggested in Figure 1 does not have a major effect on either the kinetics or the stereoselectivity of ester formation.

DISCUSSION

Kinetic Characteristics for Formation of the Alkyl-Enzyme Intermediate. The evidence presented here suggests that the rapid, pre-steady-state decrease in protein fluorescence on addition of substrate is directly associated with alkylation of the enzyme. The most interesting aspect of the alkylation reaction is the facile reversibility detected in the pre-steady-state kinetics. This particular aspect of the kinetic behavior of the intermediate led us to consider other mechanisms that might explain a reversible step associated with the decrease in fluorescence. One attractive possibility is that rapid, essentially irreversible alkylation is followed by a slower

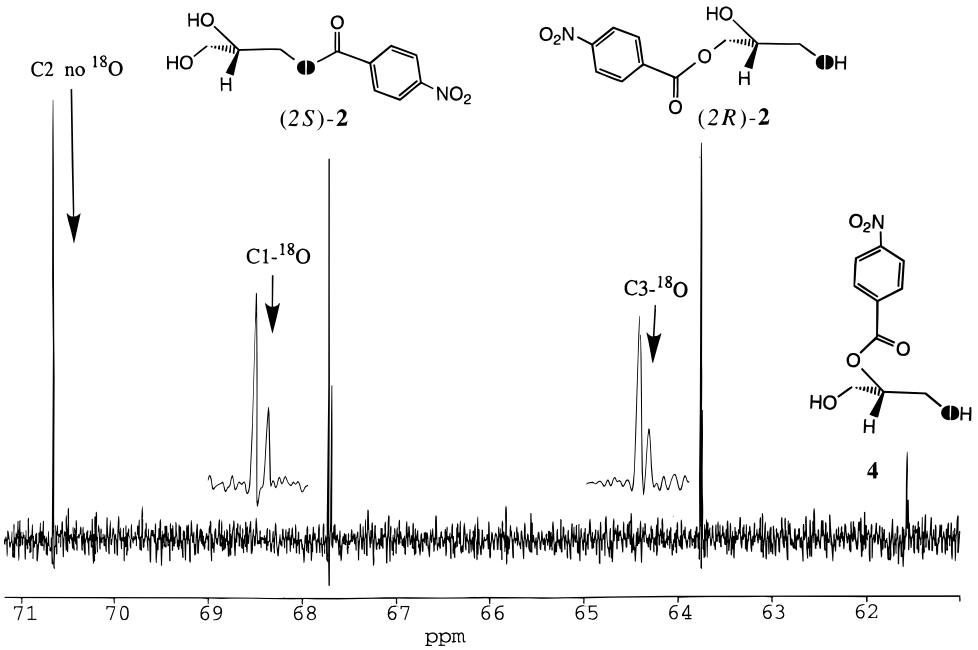

FIGURE 3: Portion of the ^{13}C NMR spectrum of the product isolated from the enzyme-catalyzed hydration of (2*R*)-**1** in the presence of 50% $H_2{}^{18}O$. The immediate product of the enzymatic hydration, (2*R*)-2, is in equilibrium with its enantiomer, (2*S*)-**2**, via the intermediate **4**. Isotopically shifted signals are observed only for the primary carbons of the glycerol backbone. The signals for the primary carbons of the rearrangement product **4** can be seen at 61.5 ppm.

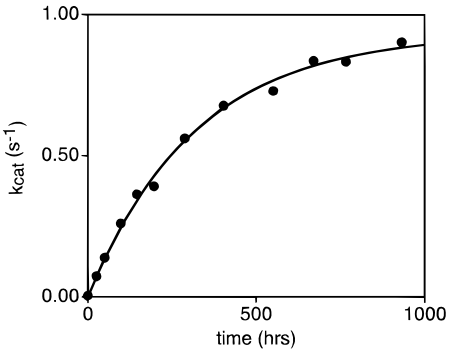

FIGURE 4: Autoactivation of the D226N mutant on incubation at pH 8.0 and 37 °C. The line is a fit of the experimental data to a single exponential with $k_{obs} = 8.6 \times 10^{-7}$ s^{-1} ($t_{1/2} = 9.3$ days) and a maximal $k_{cat} = 0.94$ s^{-1}. The return of activity was monitored by assay with **3** where the turnover number for the fully active native enzyme is 1.1 s^{-1}.

Scheme 3

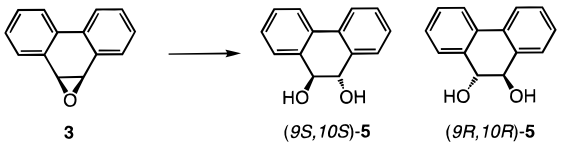

reversible conformational change that results in fluorescence quenching and leads a complex (E*−I) from which hydrolysis of the ester occurs (eq 2).

$$E + S \overset{K_s}{\rightleftharpoons} E{\cdot}S \xrightarrow{k_2} E{-}I \underset{k_{-3}}{\overset{k_3}{\rightleftharpoons}} E^*{-}I \xrightarrow{k_4} E + P \qquad (2)$$

Inasmuch as the transition states for the two half reactions are clearly different, involving stabilization of structurally different oxyanions, a significant conformational change to set up the ester for hydrolysis is certainly a reasonable possibility. However, attempts to fit the pre-steady-state and post-steady-state kinetic data to such a mechanism were not successful. The pre-steady-state kinetics therefore appear to reflect the rate of the chemical step of alkylation/dealkylation and not a rate-limiting conformational change involving k_3/k_{-3} as in eq 2.

For the mechanism described in eq 1 where $k_2 \gg k_3$ and $k_{-2} \neq 0$ the steady-state kinetic parameters are given by $k_{cat} = k_3$ and $k_{cat}/K_m = (k_2/K_s)[k_3/(k_3 + k_{-2})]$. The values of k_{cat}/K_m calculated from the pre-steady-state rate constants for (2*R*)-**1** (2.8×10^4 M^{-1} s^{-1}) and (2*S*)-**1** (1.5×10^4 M^{-1} s^{-1}) are in excellent agreement with the experimentally determined values (Table 1). It is also important to point out that the steady-state values of K_m for (2*R*)-**1** (19 μM) and (2*S*)-**1** (3.7 μM) are very much smaller than the actual dissociation constants of the substrates ($K_s \geq 2$ mM). The extensive accumulation of the intermediate in the steady-state precludes the use of K_m values as estimates of substrate dissociation constants.

Enantioselectivity and Regioselectivity of MEH. The enantioselectivity of the native enzyme toward **1** is quite instructive with respect to mechanism. First of all, the enantioselectivity is not associated with a change in the regiochemistry of the reaction. Attack of the carboxylate at the least hindered oxirane carbon is preferred in both instances as has been observed with numerous other substrates (*22*, *23*). The rates (k_2) and efficiencies (k_2/K_s) of the alkylation step for both enantiomers are comparable, and the enantioselectivity is manifest almost entirely in the rate of decomposition of the alkyl-enzyme intermediate. The change in rates of partitioning of the intermediate in both the forward and reverse direction indicates that the primary difference in the chemistry of the two enantiomers is the stability of the alkyl-enzyme intermediate as illustrated in Figure 6. The (2*S*)-enantiomer is turned over more slowly because the alkyl-enzyme intermediate is more stable than

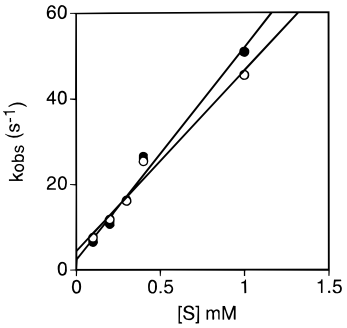

FIGURE 5: Dependence of k_{obs} for the pre-steady-state decrease in fluorescence of the W227F mutant on the concentration of (2*R*)-**1** (○) and (2*S*)-**1** (●). The lines are least-squares fits of the data to the equation $k_{obs} = k_{-2} + k_2[S]/K_s$ with the values of k_2/K_s and k_{-2} given in Table 1. It was not possible to collect data at higher substrate concentrations due to the limited solubility of **1** (ca. 1 mM).

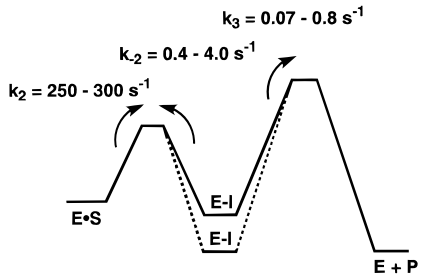

FIGURE 6: Reaction coordinate diagram for partitioning of the alkyl-enzyme intermediate formed from reaction of MEH with (2*R*)-**1** (solid line) and (2*S*)-**1** (broken line) using the rate constants in Table 1. The free energies of the E•S complexes are assumed to be equivalent. The diagram is not to scale.

the diastereomeric intermediate formed from the (2*R*)-enantiomer.

This behavior may appear to be a bit unusual when considered in the generally accepted context of the evolution of catalytic efficiency advanced by Albery and Knowles 2 decades ago (*24*). In this formalism, the most facile way to increase catalytic efficiency is through uniform binding of an intermediate and the flanking transition states. Consequently, enhanced stability of an intermediate tends to be equated with enhanced stability of the adjoined transition states. The obvious difference here is that MEH is not necessarily a highly evolved catalyst for any particular xenobiotic substrate. This is not surprising since an effective detoxication enzyme is expected to have a relatively high tolerance for substrate topology, a fact that essentially precludes the effective use of uniform binding involving distal functional groups to improve catalysis. The enhanced stability of the alkyl-enzyme intermediate formed with (2*S*)-**1** is simply due to differential binding of the intermediate, a fortuitous consequence of the stereochemistry at carbon-2.

Comments on the Acyl Migration in the Product. The relatively facile migration of the 4-nitrobenzoyl group in the monoglyceride products in the absence of enzyme is well established but has interesting implications for what could occur in the enzyme active site under the appropriate conditions. In principle, similar intramolecular rearrangements can occur in the alkyl-enzyme intermediate as illustrated in structures **6** and **7** (Scheme 4). In the specialized case of a diglyceride intermediate formed with substrates such as **1**, an acyl walk from the primary to the secondary

Scheme 4

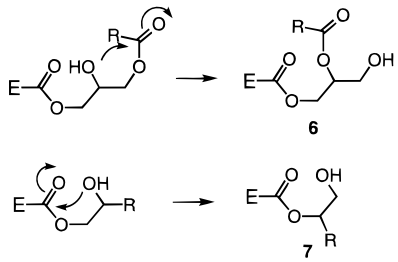

hydroxyl group is possible as illustrated in **6**. In the more general case, it is also conceivable that the enzymic acyl group may migrate as in **7**. The rate constants for acyl migration in **2** and **4** in aqueous solution are on the order of 10^{-3} s^{-1}, only slightly smaller than that for hydrolysis of the alkyl-enzyme intermediate. Given the right circumstances such rearrangements may thus compete with and complicate the hydrolytic half-reaction. Although there is no evidence for either type of migration in ester intermediates involving the native enzyme, such rearrangements are possible and may be competitive with hydrolysis particularly where hydrolysis is very slow.

Alkylation Reaction: Role of D226 in Catalysis. Sequence alignments with haloalkane dehalogenase and soluble epoxide hydrolase clearly implicate D226 as the catalytic nucleophile in MEH. The characteristics of the D226E and D226N mutants provide the first experimental support for that proposition analogous to previous studies of haloalkane dehalogenase (*25*) and the eukaryotic and microbial soluble epoxide hydrolase (*26*−*28*). The inactive D226E mutant is consistent with the essential role of D226 and further suggests that a precise environment exists for activating the carboxylate of D226 for nucleophilic attack. Even more compelling is the autoactivation of the D226N mutant to give active native enzyme. The fact that hydrolysis of the amide is accelerated compared to the pentapeptide GGNWG with the same sequence as the D226N mutant provides concrete evidence that the side chain of residue 226 is in an environment set up for addition of water to the carbonyl group of the side chain. That is to say, D226N is a semi functional mutant in that the elements required for the hydrolytic half-reaction remain intact and functional.

Alkylation Reaction: Role of W227 in Catalysis. The tryptophan residue, W125, adjoined to nucleophile D124 in haloalkane dehalogenase has been shown to be involved in formation of the alkyl-enzyme intermediate by donating a hydrogen bond from the indole NH to the Cl^- leaving group, thus providing part of the chloride ion binding site (*29*, *30*). An analogous role for W227, providing a hydrogen bond to the oxirane oxygen in the alkylation half-reaction of MEH, is ruled out by the very similar pre-steady-state kinetic behavior of the W227F mutant and native MEH. That the mutation has a modest effect on the enantioselectivity of the enzyme toward **1** and **3** suggests that this or other nearby residues may help control the substrate selectivity of MEH.

Although residues that may be involved in electrophilic activation of the oxirane oxygen remain to be elucidated, it has been proposed by others that a lysyl side chain might be involved in this aspect of catalysis (*9*, *28*, *31*). Multiple sequence alignments with other epoxide hydrolases have led Rink et al. (*28*) to propose that K173 of the *Agrobacterium*

radiobacter enzyme may serve this function. Mutation of the corresponding residue (K328) in MEH results in an enzyme with little or no catalytic activity, an observation consistent with an essential role in catalysis.[2]

ACKNOWLEDGMENT

We thank Professor Charles Kasper for supplying the pEH52 plasmid from which the expression system was constructed.

REFERENCES

1. Armstrong, R. N. (1987) *CRC Crit. Rev. Biochem. 22*, 39−88.
2. Lacourciere, G. M., and Armstrong, R. N. (1993) *J. Am. Chem. Soc. 115*, 10466−10467.
3. Tzeng, H.-F., Laughlin, L. T., Lin, S., and Armstrong, R. N. (1996) *J. Am. Chem. Soc. 118*, 9436−9437.
4. Ollis, D. L., Cheah, E., Cygler, M., Dijkstra, B., Frolow, F., Franken, S. M., Harel, M., Remington, S. J., Silman, I., Schrag, J., Sussman, J. L., Verschueren, K. H. G., and Goldman, A. (1992) *Protein Eng. 5*, 197−211.
5. Verschueren, K. H. G., Seljee, F., Rozeboom, H. J., Kalk, K. H., and Dijkstra, B. W. (1993) *Nature 363*, 693−698.
6. Janssen, D. B., Pries, F., van der Ploeg, J., Kazemier, B., Terpstra, P., and Witholt, B. (1989) *J. Bacteriol. 171*, 6791−6799.
7. Lacourciere, G. M., and Armstrong, R. N. (1994) *Chem. Res. Toxicol. 7*, 121−124.
8. Arand, M., Grant, D. F., Beetham, J. K., Friedberg, T., Oesch, F., and Hammock, B. D. (1994) *FEBS Lett. 338*, 251−256.
9. Bell, P. A., and Kasper, C. B. (1993) *J. Biol. Chem. 268*, 14011−14017.
10. Krishnan, S., Kuhn, D. G., and Hamilton, G. A. (1977) *J. Am. Chem. Soc. 99*, 812−813.
11. Porter, T., Beck, T. W., and Kasper, C. B. (1986) *Arch. Biochem. Biophys. 248*, 121−129.
12. Kunkel, T. A. (1985) *Proc. Natl. Acad. Sci. U.S.A. 82*, 488−492.
13. Armstrong, R. N., Levin, W., and Jerina, D. M. (1980) *J. Biol. Chem. 255*, 4698−4705.
14. Cleland, W. W. (1979) *Methods Enzymol. 63*, 103−138.
15. Barshop, B. A., Wrenn, R. F., and Frieden, C. (1983) *Anal. Biochem. 130*, 134−145.
16. Zimmerle, C. T., and Frieden, C. (1989) *Biochem J. 258*, 381−387.
17. Lacourciere, G. M., Vakharia, V. N., Tan, C. P., Morris, D. I., Edwards, G. H., Moos, M., and Armstrong, R. N. (1993) *Biochemistry 32*, 2610−2616.
18. Lu, A. Y. H., Ryan, D., Jerina, D. M., Daly, J. W., and Levin, W. (1975) *J. Biol. Chem. 250*, 8283−8288.
19. Lohuizen, O. E., and Verkade, P. E. (1960) *Recueil 79*, 133−159.
20. Robinson, A. B., and Tedro, S. (1973) *Int. J. Pept. Protein Res. 5*, 275−278.
21. Armstrong, R. N., Kedzierski, B., Levin, W., and Jerina, D. M. (1981) *J. Biol. Chem. 256*, 4726−4733.
22. Hanzlik, R. P., Edelman, M., Michaely, W. J., and Scott, G. (1976) *J. Am. Chem. Soc. 98*, 1952−1955.
23. Hanzlik, R. P., Heideman, S., and Smith, D. (1978) *Biochem. Biophys. Res. Commun. 82*, 310−316.
24. Albery, W. J., and Knowles, J. R. (1976) *Biochemistry 15*, 5631−5640.
25. Pries, F., Kingma, J., and Janssen, D. B. (1995) *FEBS Lett. 358*, 171−174.
26. Pinot, F., Grant, D. F., Beetham, J. K., Parker, A. G., Borhan, B., Landt, S., Jones, A. D., and Hammock, B. D. (1995) *J. Biol. Chem. 270*, 7968−7974.
27. Arand, M., Wagner, H., and Oesch, F. (1996) *J. Biol. Chem. 271*, 4223−4229.
28. Rink, R., Fennema, M., Smids, M., Dehmel, U., and Janssen, D. B. (1997) *J. Biol. Chem. 272*, 14650−14657.
29. Kennes, C., Pries, F., Krooshof, G. H., Bokma, E., Kingma, J., and Janssen, D. B. (1995) *Eur. J. Biochem*. 228, 403−407.
30. Verschueren, K. H., Kingma, J., Rozeboom, H. J., Kalk, K. H., Janssen, D. B., and Dijkstra, B. W. (1993) *Biochemistry 32*, 9031−9037.
31. Beetham, J. K., Grant, D., Arand, M., Garbarino, J., Kiyosue, T., Pinot, F., Oesch, F., Belknap, W. R., Shinozaki, K., and Hammock, B. D. (1995) *DNA Cell Biol. 14*, 61−71.

BI972737F

[2] Preliminary results (C. S. Cassidy, H.-F. Tzeng, and R. N. Armstrong, unpublished results) indicate that the K328Q mutant of MEH has an apparent k_{cat} toward **3** of $\leq 1 \times 10^{-5}$ s^{-1}. The pre-steady-state kinetics of this and related mutants need to be more extensively evaluated before the role of this lysine in the catalytic mechanism can be clearly established.